

Cite this: *RSC Adv.*, 2018, 8, 16753

# One-time sintering process to synthesize ZrO<sub>2</sub>-coated LiMn<sub>2</sub>O<sub>4</sub> materials for lithium-ion batteries†

Gang Li,<sup>a</sup> Xu Chen,<sup>a</sup> Yafei Liu,<sup>b</sup> Yanbin Chen<sup>b</sup> and Wensheng Yang<sup>a\*</sup>

Herein, different amounts of ZrO<sub>2</sub>-coated LiMn<sub>2</sub>O<sub>4</sub> materials are successfully prepared by one-time sintering ZrO<sub>2</sub>-coated Mn<sub>3</sub>O<sub>4</sub> and Li<sub>2</sub>CO<sub>3</sub>. Scanning and transmission electron microscopy results confirm that the ZrO<sub>2</sub> coating layer on the surface of Mn<sub>3</sub>O<sub>4</sub> can still be maintained on the surface of the final LiMn<sub>2</sub>O<sub>4</sub> particles even after long-term high-temperature heat-treatment. Three key factors to realize ZrO<sub>2</sub>-coated LiMn<sub>2</sub>O<sub>4</sub> materials *via* the one-time sintering process are as follows: (i) the Mn<sub>3</sub>O<sub>4</sub> precursor is coated by ZrO<sub>2</sub> in advance; (ii) the ionic radius of Zr<sup>4+</sup> is much larger than those of Mn<sup>3+</sup> and Mn<sup>4+</sup>; (iii) the pre-calcination temperature is set in the reaction temperature range between Li<sub>2</sub>CO<sub>3</sub> and Mn<sub>3</sub>O<sub>4</sub> and lower than that between Li<sub>2</sub>CO<sub>3</sub> and ZrO<sub>2</sub>. The 3 wt% ZrO<sub>2</sub>-coated LiMn<sub>2</sub>O<sub>4</sub> material exhibits excellent electrochemical properties with an initial specific discharge capacity of 118.8 mA h g<sup>-1</sup> and the capacity retention of 90.1% after 400 cycles at 25 °C and 88.9% after 150 cycles at 55 °C. Compared with the conventional coating method, the one-time sintering process to synthesize ZrO<sub>2</sub>-coated LiMn<sub>2</sub>O<sub>4</sub> materials is very simple, low-cost, environmentally friendly, and easy to scale up for large-scale industrial production, which also provides a valuable reference for preparing other coating-type cathode materials for lithium-ion batteries.

Received 14th February 2018  
Accepted 1st May 2018

DOI: 10.1039/c8ra01421c

rsc.li/rsc-advances

## Introduction

Rechargeable lithium-ion batteries (LIBs) have achieved great success as the power sources for portable electronic devices due to their high energy density and long cycle life. Recently, the demand for LIBs has been increasingly shifting from small portable power systems to electric vehicles (EVs) and large-scale energy storage systems (ESSs).<sup>1,2</sup> The safety and cost issues are mostly concerned for EVs and ESSs.<sup>3,4</sup> LiMn<sub>2</sub>O<sub>4</sub> is one of the most suitable cathode materials owing to its high abundance, low material cost, and high safety.<sup>5</sup> However, the practical application of LiMn<sub>2</sub>O<sub>4</sub> is greatly limited due to their poor cycling performance, especially at elevated temperatures (≥55 °C).<sup>6</sup> The reasons can be summarized as follows: (1) the dissolution of Mn<sup>2+</sup> from cathode to electrolyte *via* a disproportionation reaction (2Mn<sub>solid</sub><sup>3+</sup> → Mn<sub>solid</sub><sup>4+</sup> + Mn<sub>electrolyte</sub><sup>2+</sup>);<sup>7–9</sup> (2) structural transformation from cubic to tetragonal phase, induced by the Jahn–Teller distortion of Mn<sup>3+</sup>;<sup>10,11</sup> (3) the electrolyte decomposition on the electrode surface at high voltage.<sup>12</sup>

To solve the above problems, two strategies, namely the doping and coating techniques, are usually employed to improve the room-temperature (RT) and high-temperature (HT)

cycling performance of LiMn<sub>2</sub>O<sub>4</sub> materials. Partial substitution of Mn<sup>3+</sup> with other metal ions, such as Li<sup>+</sup>, Al<sup>3+</sup>, Co<sup>3+</sup>, and Cr<sup>3+</sup>, can stabilize the structure of LiMn<sub>2</sub>O<sub>4</sub> materials, which is attributed to the strong metal–oxygen bonds formed by the doping metals.<sup>5,13–15</sup> With regard to the synthetic operations, the doping elements can be easily added in the precursor-synthesizing or the raw-material-mixing processes.<sup>16–20</sup> Therefore, no extra processes are needed and the production cost would not be greatly increased.

The coating technology is another effective strategy to improve the cycling performance of LiMn<sub>2</sub>O<sub>4</sub> materials. The coating layer can protect the inner active materials from attack by the acidic species such as HF and oxidation of carbonate solvents at high voltages.<sup>21</sup> Many electrochemical inert materials<sup>12,22–24</sup> such as ZrO<sub>2</sub>, Al<sub>2</sub>O<sub>3</sub>, TiO<sub>2</sub>, AlPO<sub>4</sub>, AlF<sub>3</sub> and many coating methods<sup>6,25–29</sup> such as sol–gel, wet-coating, spray drying, atomic layer deposition (ALD) have been widely studied. Until now, the coating-type LiMn<sub>2</sub>O<sub>4</sub> materials are usually synthesized by sintering two times: the pristine LiMn<sub>2</sub>O<sub>4</sub> is firstly prepared by calcination at ~800 °C, and then the LiMn<sub>2</sub>O<sub>4</sub> is coated with some inert materials and followed by re-calcination between 400 °C and 600 °C. Although the coating techniques can effectively improve the cycling performance, they still have some drawbacks. For example, the production cost of ALD is very high, the sol–gel and spray drying methods are of high-energy consumption, and wet-coating method would generate a large amount of wastewater. Therefore, the industrial applications of the current coating techniques are greatly hindered

<sup>a</sup>State Key Laboratory of Chemical Resource Engineering, Beijing University of Chemical Technology, Beijing 100029, P. R. China. E-mail: yangws@mail.buct.edu.cn

<sup>b</sup>Beijing Easpring Material Technology Co., Ltd., Beijing 100160, P. R. China

† Electronic supplementary information (ESI) available. See DOI: 10.1039/c8ra01421c

by the complicated or high-cost coating processes.<sup>30,31</sup> Consequently, a simple, low-cost, environmental friendly, and easily scaled-up coating technique is urgent to be developed to solve the above problems.

In this work, a one-time sintering process was employed to synthesize  $\text{ZrO}_2$ -coated  $\text{LiMn}_2\text{O}_4$  materials. Scanning and high resolution transmission electron microscope (SEM and HRTEM) results clearly demonstrate that the  $\text{LiMn}_2\text{O}_4$  particles can be successfully coated by  $\text{ZrO}_2$  *via* the one-time sintering process. The electrochemical measurements demonstrate that the RT and HT cycling performances of  $\text{ZrO}_2$ -coated  $\text{LiMn}_2\text{O}_4$  materials are greatly enhanced. This one-time sintering process to synthesize  $\text{ZrO}_2$ -coated  $\text{LiMn}_2\text{O}_4$  materials is very simple, low-cost, and environmental friendly, which can promote its practical application. Besides, we systematically investigated the key influence factors in the synthesis of  $\text{ZrO}_2$ -coated  $\text{LiMn}_2\text{O}_4$  materials *via* the one-time sintering process, which can provide a valuable reference for synthesizing other coating-type cathode materials for LIBs.

## Experimental

### Material preparation

The pristine and different amounts of  $\text{ZrO}_2$ -coated  $\text{LiMn}_2\text{O}_4$  materials were synthesized by a high-temperature solid-state reaction. The shape and particle size distribution of the raw materials of  $\text{Mn}_3\text{O}_4$  (Nanjing Tianyuan Magnetic Material Co., Ltd.) and  $\text{ZrO}_2$  (Xuan Cheng Jing Rui New Material Co., Ltd.) can be seen in Fig. S1 and S2 in ESI.† The amount of  $\text{ZrO}_2$  was calculated based on the weight of the final  $\text{LiMn}_2\text{O}_4$  material. Therefore, in order to synthesize 1, 3, and 5 wt%  $\text{ZrO}_2$ -coated  $\text{LiMn}_2\text{O}_4$ , the adding amount of  $\text{ZrO}_2$  was 1.19, 3.56, and 5.93 wt% of the weight of  $\text{Mn}_3\text{O}_4$ , respectively.

The one-time sintering process to synthesize 3 wt%  $\text{ZrO}_2$ -coated  $\text{LiMn}_2\text{O}_4$  is as follows as an example: industrial grade  $\text{Mn}_3\text{O}_4$  (100 g) and nano-sized  $\text{ZrO}_2$  (3.56 g) were firstly weighed and ball-milled for 1 h, and then battery-grade  $\text{Li}_2\text{CO}_3$  (25.43 g, Shandong RuiFu Lithium Co., Ltd.) with the molar ratio of  $\text{Li} : \text{Mn} = 1.05 : 2$  was added to the above mixed materials and further ball-milled for 3 h. Note that the mass ratio of the agate balls to the raw materials is 1 : 1, and the rotational speed of the planetary ball mill is 400 rpm. The obtained mixtures of different amounts of  $\text{ZrO}_2$ -coated  $\text{Mn}_3\text{O}_4$  &  $\text{Li}_2\text{CO}_3$  was added into alumina crucible, then pre-heated at 550 °C for 5 h and calcined at 800 °C for 20 h in  $\text{O}_2$  atmosphere. Both of the heating and cooling rates are 3 °C  $\text{min}^{-1}$ . The calcined samples were crushed down and sifted through a sieve of 325 meshes, thus the final products were obtained. The step for preparing  $\text{ZrO}_2$ -coated  $\text{Mn}_3\text{O}_4$  can be ignored in the synthesis of the pristine  $\text{LiMn}_2\text{O}_4$ .

In order to investigate the influence of the blending manners of raw materials on the uniformity of the coating layer on particle surface of the final materials, stoichiometric amount of  $\text{Mn}_3\text{O}_4$ ,  $\text{Li}_2\text{CO}_3$ , and  $\text{ZrO}_2$  ( $\text{Li} : \text{Mn} = 1.05 : 2$ , molar ratio) are added and ball-milled at the same time. The detailed synthetic process can be seen in the ESI.† The obtained sample is denoted as  $\text{LMO@ZrO}_2$ . Additionally, 3 wt%  $\text{ZrO}_2$ -coated  $\text{LiMn}_2\text{O}_4$

material was also synthesized by the conventional dry coating method to compare the coating effect of two coating methods.

Besides,  $\text{SiO}_2$  and  $\text{TiO}_2$  were also used as the coating materials to synthesize different amounts of  $\text{SiO}_2$ - and  $\text{TiO}_2$ -coated  $\text{LiMn}_2\text{O}_4$  materials, respectively. The detailed synthetic process can be seen in the ESI.†

### Material characterization

The morphologies of the synthesized materials were observed using SEM (Supra 55, Zeiss, Germany) with an energy dispersive X-ray spectroscopy (EDX, EDAX, Genesis 60, Germany). The thickness of  $\text{ZrO}_2$  coating layer was measured using Auger electron spectroscopy (AES, ULVAC-PHI, AES-PHI 700, Japan). Lattice structure and surface feature of samples were investigated using HRTEM (H-800, Hitachi, Japan). Powder X-ray diffraction measurements (XRD, D/MAX 2500, Rigaku, Japan) using  $\text{Cu K}\alpha$  radiation ( $\lambda = 0.154 \text{ nm}$ ) were employed to identify the crystalline phase of the synthesized materials. XRD data were obtained in the  $2\theta$  range of 10–80°, with a step size of 0.02°, and a count time of 4 s. From the XRD data, the lattice parameters were calculated by the least-squares method. The thermal and weight changes in the synthetic process were investigated with thermogravimetric and differential thermal analysis (TG-DTA, HCT-1, China). TG-DTA measurements of the mixed materials were performed between 25 °C and 850 °C at a heating rate of 3 °C  $\text{min}^{-1}$ .

### Electrochemical measurement

The prepared powders were mixed with carbon black and polyvinylidene fluoride (PVDF) with a weight ratio of 80 : 10 : 10 in *N*-methyl-2-pyrrolidinone (NMP) to fabricate the positive electrodes. The obtained slurry was coated onto Al foil, followed by drying at 105 °C for 30 min, and roll-pressed in air. The electrodes were dried overnight at 100 °C in a vacuum oven prior to use. The areal mass loading of the active materials was  $\sim 10 \text{ mg cm}^{-2}$ . The CR2032 coin cells were assembled in an argon-filled glove box with an electrolyte of 1  $\text{mol L}^{-1}$   $\text{LiPF}_6$  in EC-DMC-DEC (1 : 1 : 1 weight ratio) solution and a separator of Celgard 2400. The cells were aged for 6 h before the charge/discharge test performed on a LAND CT2001A test system (Wuhan LAND electronics Co. Ltd., China) in the voltage range of 3.0–4.3 V (*vs.*  $\text{Li}^+/\text{Li}$ ) at 25 °C and 55 °C. The first 4 cycles were performed at 0.2C (24  $\text{mA g}^{-1}$ ), and then the following cycles were tested at 1C (120  $\text{mA g}^{-1}$ ).

## Results and discussion

As illustrated in Fig. 1, the one-time sintering process to synthesize  $\text{ZrO}_2$ -coated  $\text{LiMn}_2\text{O}_4$  materials includes two main procedures: the mixing and sintering processes. In the mixing process,  $\text{Mn}_3\text{O}_4$  and nano-sized  $\text{ZrO}_2$  are firstly ball-milled for 1 h to prepare  $\text{ZrO}_2$ -coated  $\text{Mn}_3\text{O}_4$  materials, and then the stoichiometric amount of  $\text{Li}_2\text{CO}_3$  is added to the above mixture and further ball-milled for 3 h. The purpose of the above process is to guarantee that most of  $\text{ZrO}_2$  particles are coated onto the



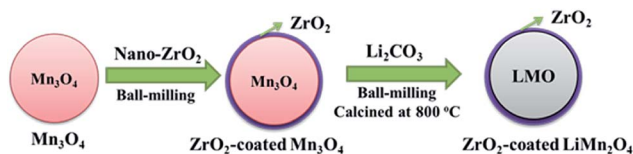


Fig. 1 Schematic illustration for the one-time sintering process to synthesize  $\text{ZrO}_2$ -coated  $\text{LiMn}_2\text{O}_4$  materials.

surface of  $\text{Mn}_3\text{O}_4$  and would not be coated onto the surface of  $\text{Li}_2\text{CO}_3$  particles.

Fig. 2 shows the SEM images of the pristine  $\text{Mn}_3\text{O}_4$  and different amounts of  $\text{ZrO}_2$ -coated  $\text{Mn}_3\text{O}_4$  materials without any heat-treatment. As shown in Fig. 2a, the pristine  $\text{Mn}_3\text{O}_4$  particles have spherical morphology and are composed of the octahedral primary particles with the particle size ranging from 100 to 200 nm. Additionally, we also notice that the  $\text{Mn}_3\text{O}_4$  particles have a rough surface and there are many particle boundaries among the primary particles. Fig. 2b–d show the SEM images of different amounts of  $\text{ZrO}_2$ -coated  $\text{Mn}_3\text{O}_4$  materials. As illustrated from the low-magnification images in Fig. 2b–d, after  $\text{ZrO}_2$  coating, the particle boundary on the surface of  $\text{Mn}_3\text{O}_4$  particles is gradually blurred with  $\text{ZrO}_2$  coating amount increasing. In addition, there are no nano-sized  $\text{ZrO}_2$  particles existing alone even when the coating amount is up to 5.93 wt%. The inset high-magnification SEM images shown in Fig. 2b–d clearly demonstrate that the surface of  $\text{Mn}_3\text{O}_4$  is uniformly coated by many  $\text{ZrO}_2$  particles with the particle size of about 30 nm. The above results indicate that nano-sized  $\text{ZrO}_2$  can be easily coated on the surface of  $\text{Mn}_3\text{O}_4$  particles through the simple dry coating method without adding any dispersant such as alcohol or water.

As shown in Fig. 3a, c, e and g, low-magnification SEM images of the pristine and different amounts of  $\text{ZrO}_2$ -coated  $\text{LiMn}_2\text{O}_4$  materials heat-treated at 800 °C for 20 h (the coating material is  $\text{ZrO}_2$ , which can be proven in the latter XRD data)

illustrate that the spherical morphology is still maintained after long-term high-temperature heat-treatment. The average particle diameter is about 10  $\mu\text{m}$ . Fig. 3b shows that the surface morphology of the pristine  $\text{LiMn}_2\text{O}_4$  is smooth and clean. In contrast, the surfaces of the coated  $\text{LiMn}_2\text{O}_4$  become rough and are covered with small particles, as shown in Fig. 3d, f and h. The coating layer becomes more and more obviously with the  $\text{ZrO}_2$  coating amount increasing from 1 to 5 wt%, which demonstrates that the coating layer is still maintained even after having been heat-treated at 800 °C for 20 h.

Lattice structure of the coating layer on  $\text{LiMn}_2\text{O}_4$  particles was investigated by HRTEM. As illustrated in Fig. 4a, HRTEM images show that there is a film-like layer as we speculate in SEM images. Fig. 4b and d show that the measured interplanar distances of the coating layer of 3 wt%  $\text{ZrO}_2$ -coated  $\text{LiMn}_2\text{O}_4$  and nano-sized  $\text{ZrO}_2$  heat-treated at 800 °C for 20 h are around 0.218 nm, respectively, which matches well to the (121) plane of  $\text{ZrO}_2$  with monoclinic crystal system. Therefore, we can draw a conclusion that the coating layer on the surface of  $\text{LiMn}_2\text{O}_4$  particles is  $\text{ZrO}_2$ .

Fig. 5b–d shows elemental mapping studies on 3 wt%  $\text{ZrO}_2$ -coated  $\text{LiMn}_2\text{O}_4$  particles. It is clear that the presence of Mn, Zr,

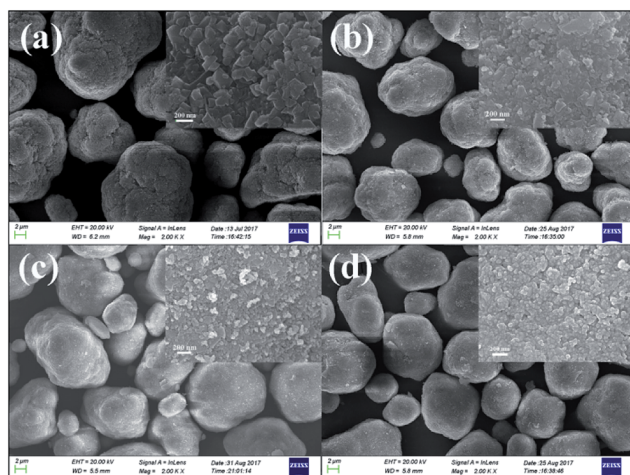


Fig. 2 SEM images of (a) the pristine  $\text{Mn}_3\text{O}_4$  and (b) 1.19 wt%, (c) 3.56 wt%, (d) 5.93 wt%  $\text{ZrO}_2$ -coated  $\text{Mn}_3\text{O}_4$  without any heat-treatment. The insets are the corresponding SEM images at high magnification.

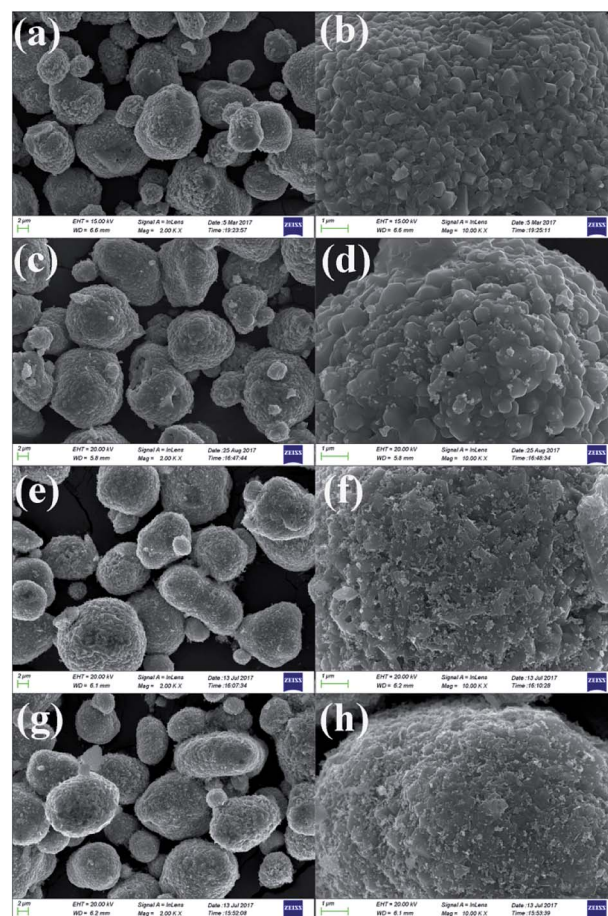


Fig. 3 SEM images of (a and b) the pristine  $\text{LiMn}_2\text{O}_4$ , (c and d) 1 wt%, (e and f) 3 wt%, and (g and h) 5 wt%  $\text{ZrO}_2$ -coated  $\text{LiMn}_2\text{O}_4$  obtained by calcining 0, 1.19, 3.56, and 5.93 wt%  $\text{ZrO}_2$ -coated  $\text{Mn}_3\text{O}_4$  &  $\text{Li}_2\text{CO}_3$  mixtures at 800 °C for 20 h.





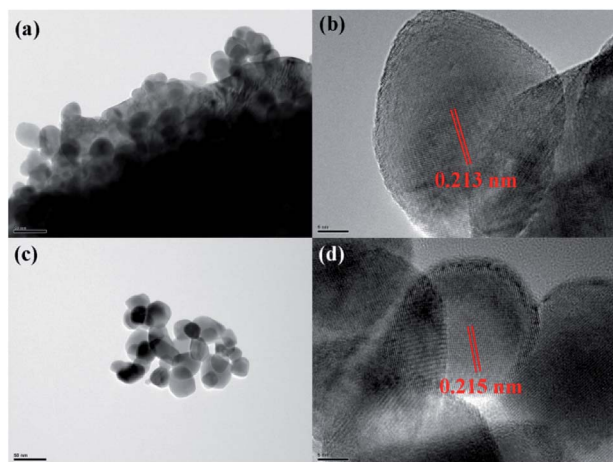


Fig. 4 HRTEM images of (a and b) 3 wt%  $\text{ZrO}_2$ -coated  $\text{LiMn}_2\text{O}_4$  and (c and d) nano-sized  $\text{ZrO}_2$  heat-treated at 800 °C for 20 h.

and O are homogenous within  $\text{LiMn}_2\text{O}_4$  particles, and the  $\text{ZrO}_2$  coating layer is uniformly distributed on the surface of  $\text{LiMn}_2\text{O}_4$  particles.

In order to confirm the extent of inter-diffusion between Zr and Mn ions in the process of high-temperature heat-treatment, EDX was used to measure the Zr/Mn atomic ratio in the particles before and after high-temperature calcination. As illustrated in Fig. 6b, the atomic ratio of Zr/Mn in 3.56 wt%  $\text{ZrO}_2$ -coated  $\text{Mn}_3\text{O}_4$  particle is 0.079/99.921. As to the final product of 3.0 wt%  $\text{ZrO}_2$ -coated  $\text{LiMn}_2\text{O}_4$  (Fig. 6d), the atomic ratio of Zr/Mn is 0.071/99.929, which is slightly lower than that of 3.56 wt%  $\text{ZrO}_2$ -coated  $\text{Mn}_3\text{O}_4$  particle. If all of Zr ions are diffused into the bulk  $\text{LiMn}_2\text{O}_4$  particles, the atomic ratio of Zr/Mn would be 0.022/99.978. Therefore, we can draw a definite conclusion that the inter-diffusion between Zr and Mn ions is very little.

In order to investigate the  $\text{ZrO}_2$  coating thickness, the theoretical value was firstly calculated. The calculation method can be seen in Fig. S3 in ESI.† The theoretical coating thickness of 1,

3, and 5 wt%  $\text{ZrO}_2$ -coated  $\text{LiMn}_2\text{O}_4$  materials is 12.2, 36.6, and 61.0 nm, respectively. AES was also employed to measure the actual coating thickness of different amounts of  $\text{ZrO}_2$ -coated  $\text{LiMn}_2\text{O}_4$  materials. From Fig. 7a, c and e, the peaks indexed to Zr1 can be easily observed on the top surface of 1, 3, and 5 wt%  $\text{ZrO}_2$ -coated  $\text{LiMn}_2\text{O}_4$  materials. As the  $\text{Ar}^+$  etching depth increases, the peak intensity of Zr1 decreases, while that of Mn1, Mn2, and Mn3 increases. When the etching depth reaches 192, 374, and 635 nm for 1, 3, and 5 wt%  $\text{ZrO}_2$ -coated  $\text{LiMn}_2\text{O}_4$  samples, though the Zr1 peak intensities are weak, they can still be observed, indicating that some Zr ions have diffused into the crystal lattice of  $\text{LiMn}_2\text{O}_4$ .

As illustrated in Fig. 7b, d and f, the changing trend of the atomic concentration of Zr and Mn can be divided into three stages: in the first stage (stage-I), the atomic concentration of Zr and Mn changes little, so the etching depth in stage-I can represent the thickness of  $\text{ZrO}_2$  coating layer. Therefore, it can be estimated from Fig. 7b, d and f that the coating thickness of 1, 3, and 5 wt%  $\text{ZrO}_2$ -coated  $\text{LiMn}_2\text{O}_4$  samples are 32, 42, and 75 nm, respectively. The measured thickness of the coating layer is slightly bigger than the theoretical value; the main reason is that the actual density of  $\text{ZrO}_2$  is reduced due to the nano-crystallization of particles. Since  $\text{ZrO}_2$  is a granular material, not a film material, so the surface coverage will be incomplete if the coating amount is small. As  $\text{ZrO}_2$  coating amount increases, the surface coverage becomes completely, and then the coating thickness will increase proportionally with the increase of  $\text{ZrO}_2$  coating amount. Considering that the coating thickness of 3 wt%  $\text{ZrO}_2$ -coated  $\text{LiMn}_2\text{O}_4$  sample is only 10 nm bigger than that of 1 wt%  $\text{ZrO}_2$ -coated sample, and the ratio of the coating thickness between 5 wt% and 3 wt% coating amount is 1.786, which is very close to 5 : 3. So, it is speculated that the surface coverage for 1 wt%  $\text{ZrO}_2$  coating amount is not complete. As the  $\text{ZrO}_2$  coating amount is  $\geq 3$  wt%, the surface coverage becomes completely, which means that the “break-through” loading to have a complete coverage should be 3 wt%. In the second stage (stage-II), the atomic concentration of Zr

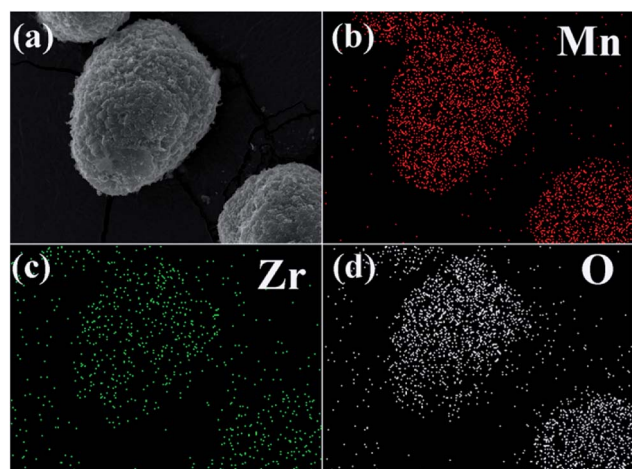


Fig. 5 (a) SEM image of 3 wt%  $\text{ZrO}_2$ -coated  $\text{LiMn}_2\text{O}_4$  and the corresponding elemental mapping of (b) Mn, (c) Zr, and (d) O.

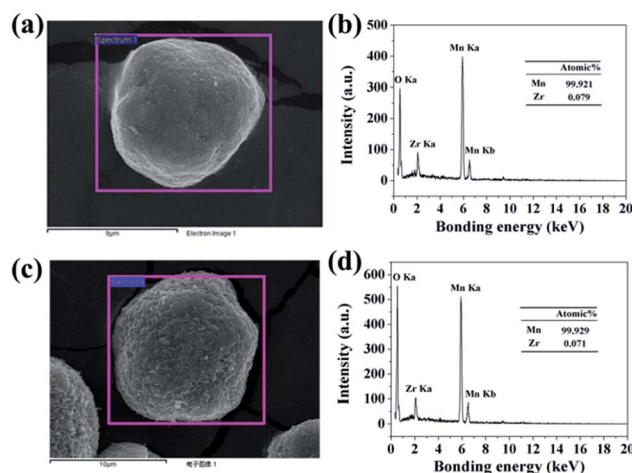


Fig. 6 (a) SEM image of 3.56 wt%  $\text{ZrO}_2$ -coated  $\text{Mn}_3\text{O}_4$  and (b) its corresponding EDX spectroscopy. (c) SEM image of 3.0 wt%  $\text{ZrO}_2$ -coated  $\text{LiMn}_2\text{O}_4$  and (d) its corresponding EDX spectroscopy.



drastically decreases and that of Mn rapidly increases, indicating that Zr ions have diffused into the crystal lattice in the surficial layer of  $\text{LiMn}_2\text{O}_4$  particles to form a  $\text{LiMn}_{2-x}\text{Zr}_x\text{O}_4$  phase. According to Fig. 7b, d and f, the thickness of  $\text{LiMn}_{2-x}\text{Zr}_x\text{O}_4$  layer for 1, 3, and 5 wt%  $\text{ZrO}_2$ -coated  $\text{LiMn}_2\text{O}_4$  samples are estimated to be 92, 158, and 325 nm, respectively, indicating that more  $\text{ZrO}_2$  content makes more Zr ions diffuse into  $\text{LiMn}_2\text{O}_4$  particles. In the third stage (stage-III), the atomic concentration of Zr is very low and changes very little with the etching depth increasing, indicating that it is very difficult for all of Zr ions to completely diffuse into the crystal lattice of  $\text{LiMn}_2\text{O}_4$  particles. From the atomic concentration of Zr in the inner part of  $\text{LiMn}_2\text{O}_4$  particles, we can obtain that some Zr ions have been doped to form a  $\text{LiMn}_{2-x}\text{Zr}_x\text{O}_4$  phase ( $0.01 \leq x \leq 0.02$ ).

The SEM, HRTEM, EDX, and AES results show that the  $\text{LiMn}_2\text{O}_4$  particles can be successfully coated by  $\text{ZrO}_2$  *via* the one-time sintering process. This coating method is very easy to be scaled up and can be used to prepare other coating-type cathode materials. However, the successful synthesis of  $\text{ZrO}_2$ -coated  $\text{LiMn}_2\text{O}_4$  *via* the one-time sintering process is just a specific example. In order to make this method more universal, we systematically studied what factors are essential to guarantee its success.

First of all, the blending manner of raw materials may be one of the key factors. In the preceding experiments, the  $\text{Mn}_3\text{O}_4$  precursor was coated with nano-sized  $\text{ZrO}_2$  in advance, and then  $\text{Li}_2\text{CO}_3$  was added and further ball-milled for 3 h. Herein, we made an adjustment to the blending manner as below. Three

raw materials of  $\text{Mn}_3\text{O}_4$ ,  $\text{Li}_2\text{CO}_3$ , and  $\text{ZrO}_2$  (the amount of  $\text{ZrO}_2$  is 3.56 wt% of the weight of  $\text{Mn}_3\text{O}_4$ ) were ball-milled simultaneously, and then the mixture was preheated at 550 °C for 5 h and then calcined at 800 °C for 20 h. The as-prepared material is denoted as  $\text{LMO@ZrO}_2$  and deemed as a control sample. SEM images of  $\text{LMO@ZrO}_2$  are illustrated in Fig. S4(a and b).† It can be seen that there is very small amount of  $\text{ZrO}_2$  observed on the surface of the  $\text{LiMn}_2\text{O}_4$  particles. However, as illustrated in Fig. S4(c and d),† a large number of  $\text{ZrO}_2$  particles can be successfully coated onto the  $\text{LiMn}_2\text{O}_4$  particles through calcining the mixture of  $\text{Li}_2\text{CO}_3$  and  $\text{ZrO}_2$ -coated  $\text{Mn}_3\text{O}_4$ . According to the above comparison results, a definite conclusion can be drawn: only the precursor is coated with the coating material beforehand, can the coating material be uniformly coated onto the surface of the final particles *via* the one-time sintering process. Besides, it can also be seen from Fig. S4(e and f)† that the coating uniformity of the one-time sintering process is similar to that of the conventional coating method.

The second key factor may be choosing a suitable coating material. According to the diffusion theory, among the various physicochemical properties of the coating materials, the ionic radius may play an important role.<sup>32</sup> In order to prove the above assumption, two other metal ions of  $\text{Ti}^{4+}$  and  $\text{Si}^{4+}$  are chosen to synthesize different amounts of  $\text{SiO}_2$ - and  $\text{TiO}_2$ -coated  $\text{LiMn}_2\text{O}_4$  materials *via* the one-time sintering process. Unexpectedly, the result obtained from Fig. S6–S9† demonstrates that  $\text{SiO}_2$ - and  $\text{TiO}_2$ -coated  $\text{LiMn}_2\text{O}_4$  materials cannot be successfully synthesized by the one-time sintering process, which indicates that it is easy for  $\text{Si}^{4+}$  and  $\text{Ti}^{4+}$  to diffuse into the bulk  $\text{LiMn}_2\text{O}_4$  crystals at 800 °C. In order to compare the ionic radius difference among  $\text{Mn}^{3+}$ ,  $\text{Mn}^{4+}$ ,  $\text{Zr}^{4+}$ ,  $\text{Si}^{4+}$ , and  $\text{Ti}^{4+}$ , their ionic radii are shown in Fig. 8. It is seen that  $\text{Zr}^{4+}$  has a much larger ionic radius than  $\text{Mn}^{3+}$  and  $\text{Mn}^{4+}$ . While, the ionic radius of  $\text{Si}^{4+}$  is much smaller than those of  $\text{Mn}^{3+}$  and  $\text{Mn}^{4+}$ , and the ionic radius of  $\text{Ti}^{4+}$  is between those of  $\text{Mn}^{3+}$  and  $\text{Mn}^{4+}$ . From the comparable results of  $\text{ZrO}_2$ ,  $\text{SiO}_2$ , and  $\text{TiO}_2$  coating layers after heat-treatment at 800 °C, we can conclude that the successful synthesis of  $\text{ZrO}_2$ -coated  $\text{LiMn}_2\text{O}_4$  *via* the one-time sintering process is probably due to the much larger ionic radius of  $\text{Zr}^{4+}$  than those of  $\text{Mn}^{3+}$  and  $\text{Mn}^{4+}$ . Therefore, the ionic radius is also

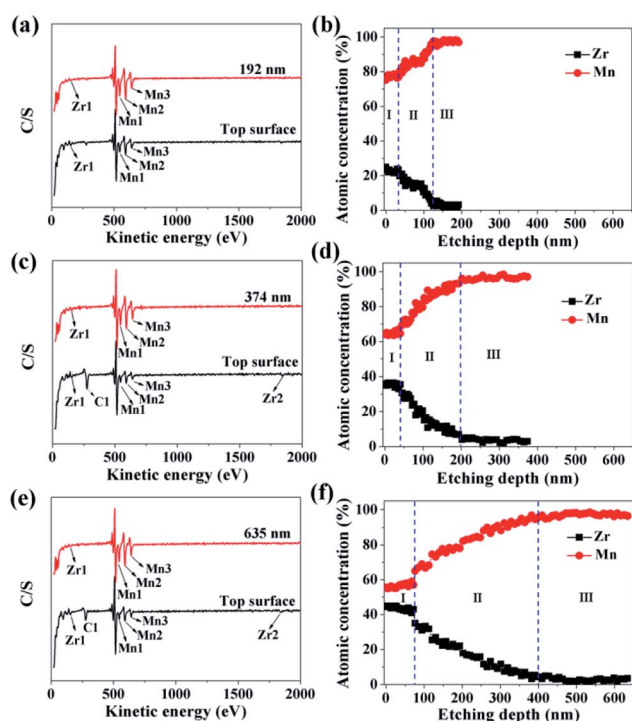


Fig. 7 AES spectroscopies of (a) 1 wt%, (c) 3 wt%, and (e) 5 wt%  $\text{ZrO}_2$ -coated  $\text{LiMn}_2\text{O}_4$ . Atomic concentration of Zr and Mn as a function of the etching depth: (b) 1 wt%, (d) 3 wt%, and (f) 5 wt%  $\text{ZrO}_2$ -coated  $\text{LiMn}_2\text{O}_4$ .

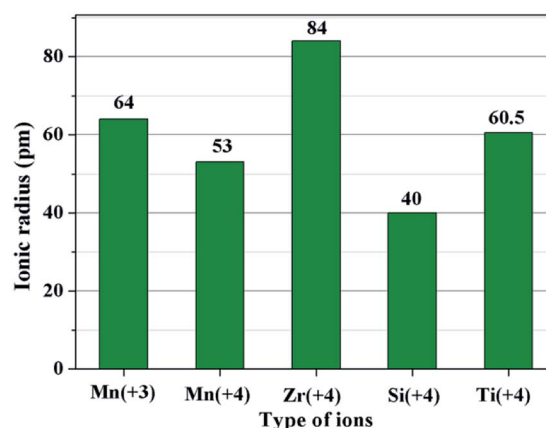


Fig. 8 The ionic radii of five types of ions:  $\text{Mn}^{3+}$ ,  $\text{Mn}^{4+}$ ,  $\text{Zr}^{4+}$ ,  $\text{Si}^{4+}$ , and  $\text{Ti}^{4+}$ .

a crucial factor to realize the coating-type materials *via* the one-time sintering process.

The third key factor should be the choice of the pre-calcination temperature. If the reaction between  $\text{Li}_2\text{CO}_3$  and  $\text{ZrO}_2$  is ahead of that  $\text{Li}_2\text{CO}_3$  and  $\text{Mn}_3\text{O}_4$ , the coating material may be  $\text{Li}_2\text{ZrO}_3$  and not  $\text{ZrO}_2$ , thus some extra  $\text{Li}_2\text{CO}_3$  will be consumed in vain and the loss of the specific discharge capacity of  $\text{LiMn}_2\text{O}_4$  will be more seriously. In order to choose a suitable pre-calcination temperature, TG-DTA was performed to reveal the reaction process between  $\text{Li}_2\text{CO}_3$  and  $\text{ZrO}_2$ -coated  $\text{Mn}_3\text{O}_4$  and the result is shown in Fig. 9. For the mixture of  $\text{Li}_2\text{CO}_3$  and  $\text{Mn}_3\text{O}_4$ , the reaction temperature range is between 457 °C and 600 °C. While for the mixture of  $\text{Li}_2\text{CO}_3$  and  $\text{ZrO}_2$ , the reaction temperature range is between 582 °C and 712 °C. Besides, it is also noticed that when the  $\text{Mn}_3\text{O}_4$  is coated with  $\text{ZrO}_2$  beforehand, the starting reaction temperature between  $\text{Li}_2\text{CO}_3$  and  $\text{Mn}_3\text{O}_4$  is postponed by 43 °C to 500 °C. This is because  $\text{Li}^+$  must pass through the  $\text{ZrO}_2$  coating layer and then can react with  $\text{Mn}_3\text{O}_4$  to form  $\text{LiMn}_2\text{O}_4$ . Although there is overlap in the reaction temperature range between the mixtures of  $\text{Li}_2\text{CO}_3$  &  $\text{ZrO}_2$ -coated  $\text{Mn}_3\text{O}_4$  and  $\text{Li}_2\text{CO}_3$  &  $\text{ZrO}_2$ , it is probably that  $\text{Li}_2\text{CO}_3$  would react only with  $\text{Mn}_3\text{O}_4$  and not with  $\text{ZrO}_2$  if the pre-calcination temperature is set at 550 °C.

Influence of the sintering temperature and time on the crystal structure and performance of the pristine  $\text{LiMn}_2\text{O}_4$  and different amounts of  $\text{ZrO}_2$ -coated  $\text{LiMn}_2\text{O}_4$  materials were investigated in detail. As illustrated in Fig. S10 and S11,<sup>†</sup> the diffraction peaks of  $\text{ZrO}_2$  can always be observed between 550 °C to 850 °C, which shows that the coating layer is indeed  $\text{ZrO}_2$  and the coating layers do not disappear even after long-term high-temperature calcination. Fig. S12<sup>†</sup> shows the influence of sintering temperature on cyclic performance of the pristine  $\text{LiMn}_2\text{O}_4$ , and the optimal synthesizing temperature is 800 °C. Fig. S13<sup>†</sup> demonstrates that the discharge capacity slightly increases and the capacity retention slightly decreases with the sintering time increasing. Therefore, the synthesizing condition of the pristine  $\text{LiMn}_2\text{O}_4$  and different amounts of  $\text{ZrO}_2$ -coated  $\text{LiMn}_2\text{O}_4$  materials is set at 800 °C for 20 h.

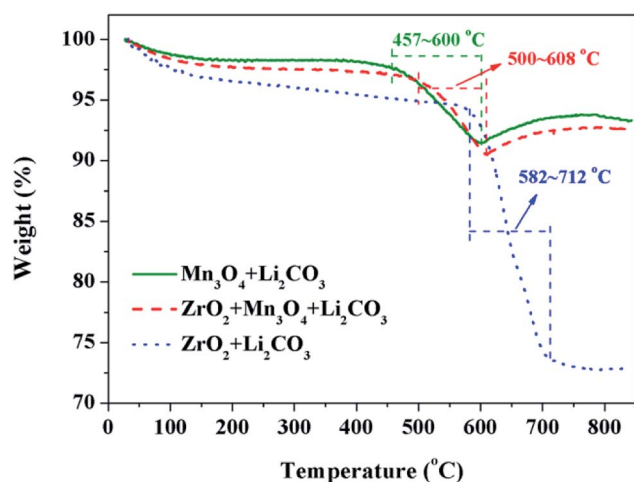


Fig. 9 TG curves of the raw material mixtures with a heating rate of 3 °C min<sup>-1</sup> in air.

The XRD patterns of the pristine and different amounts of  $\text{ZrO}_2$ -coated  $\text{LiMn}_2\text{O}_4$  materials calcined at 800 °C for 20 h are shown in Fig. 10a. The major diffraction peaks of the pristine  $\text{LiMn}_2\text{O}_4$  are in good agreement with that obtained from JCPDF file no. 35-0782, corresponding to the cubic spinel structure with  $Fd\bar{3}m$  space group. For the 1 wt%  $\text{ZrO}_2$ -coated  $\text{LiMn}_2\text{O}_4$  sample, there is no diffraction peaks corresponding to  $\text{ZrO}_2$  observed in the XRD pattern, this is because the  $\text{ZrO}_2$  amount is too low to be detected. As expected, the impurity phase of  $\text{ZrO}_2$  is obviously observed with the coating amount increasing to 3 wt% and 5 wt%, which demonstrates that most of  $\text{ZrO}_2$  do not react with  $\text{Li}_2\text{CO}_3$ . A suitable pre-calcination temperature can guarantee that  $\text{Li}_2\text{CO}_3$  does not react with  $\text{ZrO}_2$  to form  $\text{Li}_2\text{ZrO}_3$ , which leads to two advantages as below: (i) the weight of the coating layer is not further increased, which will not greatly reduce the specific discharge capacity of the final products; (ii) extra  $\text{Li}_2\text{CO}_3$  won't be consumed in vain. Therefore, the suitable pre-calcination temperature is the key factor to determine the chemical compositions of the coating materials.

Furthermore, the lattice parameter  $a$  ( $= b = c$ ) is also calculated from the XRD data and the results are shown in Fig. 10b. It is interesting that the lattice parameter of  $\text{ZrO}_2$ -coated  $\text{LiMn}_2\text{O}_4$  materials is slightly smaller than that of the pristine  $\text{LiMn}_2\text{O}_4$  material. The reason is probably that after heat-treatment at such high temperature of 800 °C for 20 h,

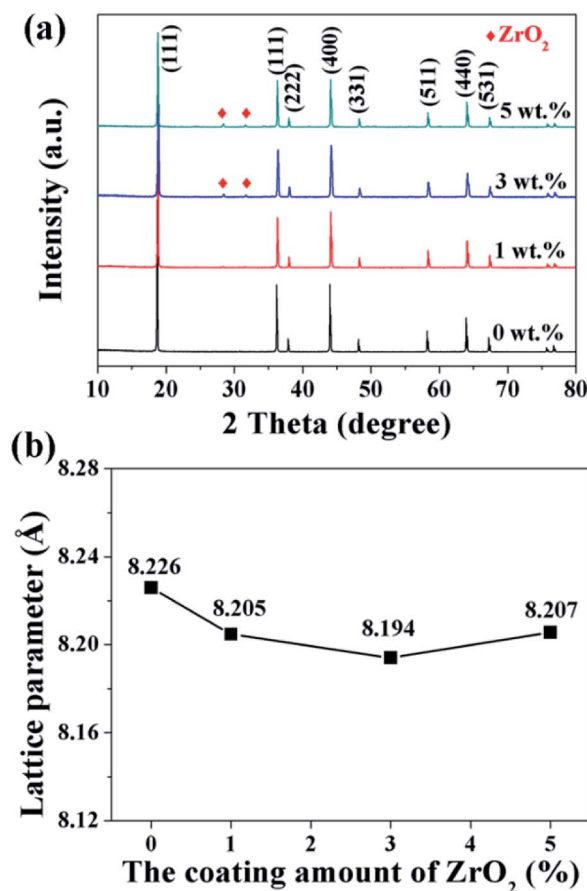


Fig. 10 (a) XRD patterns and (b) the lattice parameters of 1, 3, and 5 wt%  $\text{ZrO}_2$ -coated  $\text{LiMn}_2\text{O}_4$  materials.



a small fraction of  $\text{Zr}^{4+}$  diffuses into the spinel lattice of the bulk  $\text{LiMn}_2\text{O}_4$  to partial substitute the site of  $\text{Mn}^{4+}$ . Ionic radius of  $\text{Zr}^{4+}$  is much bigger than that of  $\text{Mn}^{4+}$ , the lattice constant should be bigger if  $\text{Zr}^{4+}$  ions substitute the site of  $\text{Mn}^{4+}$  in the spinel. But the fact is on the contrary. Actually, the lattice constant of spinel  $\text{LiMn}_2\text{O}_4$  crystal is not only related to the ionic radius, but also related to the M–O bond energy.<sup>33</sup> The  $\Delta_f G^\ominus(\text{ZrO}_2)$  and  $\Delta_f G^\ominus(\text{MnO}_2)$  is  $-1042.8 \text{ kJ mol}^{-1}$  and  $-465.1 \text{ kJ mol}^{-1}$ , respectively. The  $\Delta_f G^\ominus(\text{ZrO}_2)$  is much more negative than  $\Delta_f G^\ominus(\text{MnO}_2)$ , which can deduce that bond energy of Zr–O is much stronger than Mn–O and the crystal volume shrinks. Therefore, the structure with  $\text{Zr}^{4+}$  doping is more compact and has smaller lattice constant. Besides, the lattice parameter changes little with  $\text{ZrO}_2$  content increasing from 1 wt% to 5 wt%, the reason is that the doping content of  $\text{Zr}^{4+}$  in the inner part of  $\text{LiMn}_2\text{O}_4$  is almost constant, no matter the  $\text{ZrO}_2$  coating amount is 1 wt%, 3 wt% or 5 wt%. It implies that the upper limit of the actual  $\text{Zr}^{4+}$  amounts diffusing into the spinel lattice of  $\text{LiMn}_2\text{O}_4$  is very small, primarily because the ionic radius of  $\text{Zr}^{4+}$  is much larger than that of  $\text{Mn}^{4+}$ .

The electrochemical properties of the pristine  $\text{LiMn}_2\text{O}_4$  and different amounts of  $\text{ZrO}_2$ -coated  $\text{LiMn}_2\text{O}_4$  materials were studied in the voltage range of 3.0–4.3 V at 25 °C and 55 °C. Fig. 11a shows the initial charge–discharge curves of different amounts of  $\text{ZrO}_2$ -coated  $\text{LiMn}_2\text{O}_4$  materials at a current rate of  $24 \text{ mA g}^{-1}$  corresponding to 0.2C. It can be seen that all discharge curves have two voltage plateaus at approximately 3.95 V and 4.1 V, which is typical for  $\text{LiMn}_2\text{O}_4$  and its variants. The two voltage plateaus indicate that the extraction (and subsequent re-insertion) of lithium ions from tetrahedral sites occurs in two stages. The pristine  $\text{LiMn}_2\text{O}_4$  material delivers the highest specific discharge capacity of  $124.4 \text{ mA h g}^{-1}$  with the initial coulombic efficiency of 97.6%. The specific discharge capacities of  $\text{ZrO}_2$ -coated  $\text{LiMn}_2\text{O}_4$  materials decrease with the  $\text{ZrO}_2$  coating amount increasing. The initial discharge capacity of 1, 3, and 5 wt%  $\text{ZrO}_2$ -coated  $\text{LiMn}_2\text{O}_4$  is 121.5, 118.8, and  $115.6 \text{ mA h g}^{-1}$  with the initial coulombic efficiency of 96.4, 96.7, and 96.1%, respectively. The RT and HT cycling performance of the pristine and different amounts of  $\text{ZrO}_2$ -coated  $\text{LiMn}_2\text{O}_4$  materials is evaluated with the current density of  $120 \text{ mA g}^{-1}$  corresponding to 1C and the results are shown in Fig. 11b and c. At 25 °C, the initial specific discharge capacity of 0, 1, 3, and 5 wt%  $\text{ZrO}_2$ -coated  $\text{LiMn}_2\text{O}_4$  materials is 121.3, 118.3, 115.2, and  $109.6 \text{ mA h g}^{-1}$  with the 400<sup>th</sup> capacity retention of 79.2, 84.7, 90.1, and 87.5%, respectively. As the test temperature increases to 55 °C, the pristine  $\text{LiMn}_2\text{O}_4$  shows severe capacity loss with the capacity retention of 67.0% after 150 cycles. While the specific discharge capacity of 1, 3, and 5 wt%  $\text{ZrO}_2$ -coated  $\text{LiMn}_2\text{O}_4$  after 150 cycles is 94.1, 102.8, and  $101.7 \text{ mA h g}^{-1}$  with the capacity retention of 79.5, 88.9, and 92.9%, respectively. Compared with the pristine  $\text{LiMn}_2\text{O}_4$ , though the specific discharge capacities of  $\text{ZrO}_2$ -coated  $\text{LiMn}_2\text{O}_4$  decrease, their cycling performance is greatly improved. By comparison of the comprehensive electrochemical performance, the 3 wt% coating amount is preferred, because it has a relatively high specific discharge capacity and an excellent cycling performance.

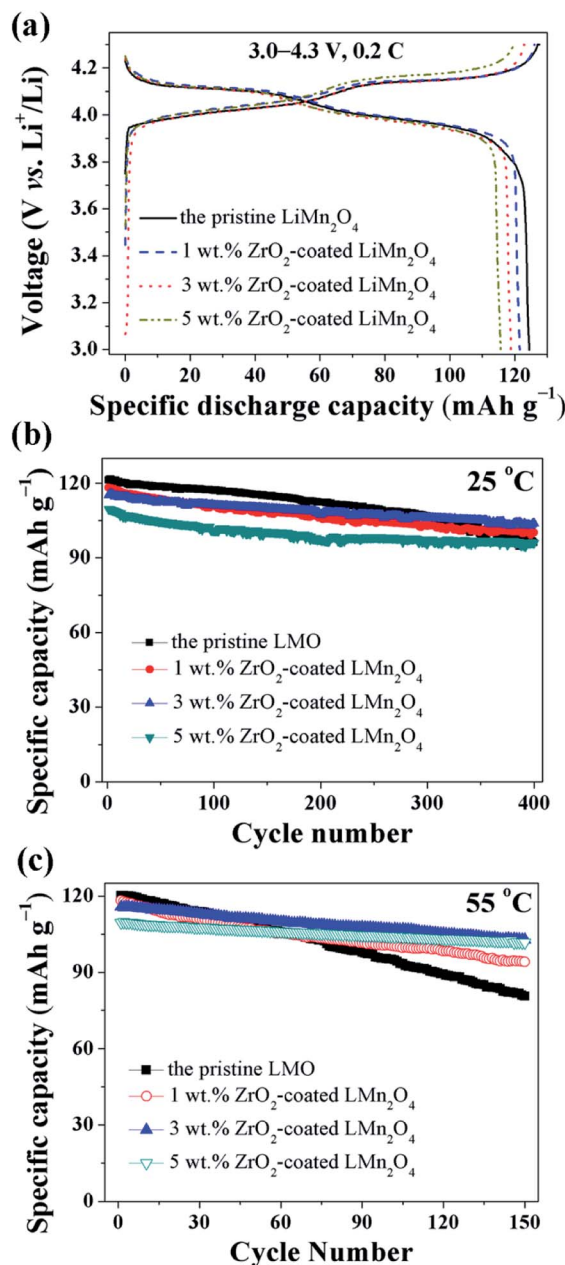


Fig. 11 (a) The charge–discharge curves of 1, 3, and 5 wt%  $\text{ZrO}_2$ -coated  $\text{LiMn}_2\text{O}_4$  materials with the current rate of 0.2C. The cycling performance of 1, 3, and 5 wt%  $\text{ZrO}_2$ -coated  $\text{LiMn}_2\text{O}_4$  materials tested at (b) 25 °C and (c) 55 °C at 1C.

The enhanced cycling performance should be mainly contributed to the  $\text{ZrO}_2$  coating layer, which can suppress the  $\text{Mn}^{2+}$  dissolution from  $\text{LiMn}_2\text{O}_4$  cathode into the electrolyte. In order to measure the  $\text{Mn}^{2+}$  dissolution, 0.3 g cathode materials were added into 10 mL electrolyte and stored for 7 days at 60 °C, and then the  $\text{Mn}^{2+}$  concentration was tested by ICP. As illustrated in Fig. 12, the  $\text{Mn}^{2+}$  concentration in electrolyte for the pristine  $\text{LiMn}_2\text{O}_4$  is  $0.75 \text{ mmol L}^{-1}$ . In comparison, the  $\text{Mn}^{2+}$  concentrations in electrolyte for 1, 3, and 5 wt%  $\text{ZrO}_2$ -coated  $\text{LiMn}_2\text{O}_4$  materials drops quickly to 0.62, 0.25, and  $0.2 \text{ mmol L}^{-1}$ , which proves that the  $\text{ZrO}_2$  coating layer can greatly inhibit

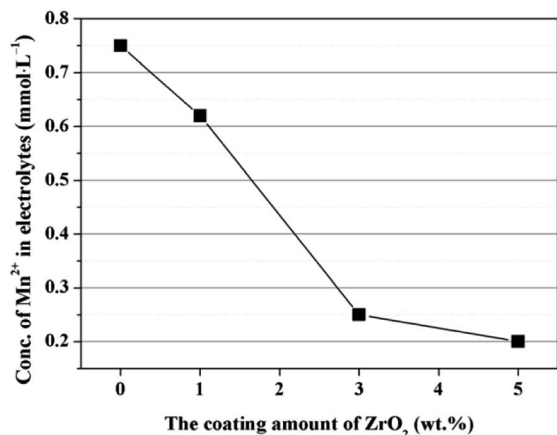


Fig. 12 Concentration of Mn<sup>2+</sup> in the electrolyte as a function of the coating amounts of ZrO<sub>2</sub>.

the Mn<sup>2+</sup> dissolution from the active material into the electrolyte.

In order to investigate the stability of the ZrO<sub>2</sub> coating layer, SEM and XRD were used to characterize the morphology and crystal structure of 3 wt% ZrO<sub>2</sub>-coated LiMn<sub>2</sub>O<sub>4</sub> electrode post electrochemical testing, and the results are shown in Fig. S14 and S15.† Based on the analysis of SEM and XRD data, we can conclude that the ZrO<sub>2</sub> coating layer on the surface of LiMn<sub>2</sub>O<sub>4</sub> particles is very stable to the volume changes brought by the long-term charge–discharge processes. The reason is probably that the coating layer calcined at 800 °C is very rigid and stable.

## Conclusions

In summary, different amounts of ZrO<sub>2</sub>-coated LiMn<sub>2</sub>O<sub>4</sub> materials are successfully synthesized *via* a one-time sintering process. Three key factors to realize ZrO<sub>2</sub>-coated LiMn<sub>2</sub>O<sub>4</sub> materials are as follows: (i) the Mn<sub>3</sub>O<sub>4</sub> precursor is coated by nano-sized ZrO<sub>2</sub> in advance; (ii) the ionic radius of Zr<sup>4+</sup> is much larger than those of Mn<sup>3+</sup> and Mn<sup>4+</sup>; (iii) the pre-calcination temperature is set in the reaction temperature range between Li<sub>2</sub>CO<sub>3</sub> and Mn<sub>3</sub>O<sub>4</sub> and lower than that between Li<sub>2</sub>CO<sub>3</sub> and ZrO<sub>2</sub>. The as-prepared 3 wt% ZrO<sub>2</sub>-coated LiMn<sub>2</sub>O<sub>4</sub> material exhibits an excellent electrochemical performance with the initial specific discharge capacity of 118.8 mA h g<sup>-1</sup> at 0.2C and the capacity retention of 90.1% after 400 cycles at 25 °C and 88.9% after 150 cycles at 55 °C at 1C. The enhancement of the cycling performance is mainly contributed to the ZrO<sub>2</sub> coating layer which can suppress the side reactions between LiMn<sub>2</sub>O<sub>4</sub> and the electrolyte. Most significantly, the one-time sintering process to synthesize ZrO<sub>2</sub>-coated LiMn<sub>2</sub>O<sub>4</sub> materials is very simple, low-cost, environmental friendly, and easy for large-scale industrial production, so as to promote its practical application and provide a valuable reference for synthesizing other coating-type cathode materials for LIBs.

## Conflicts of interest

There are no conflicts to declare.

## Acknowledgements

This work was financially supported by the National Natural Science Foundation of China (U1407118 and 51272020).

## Notes and references

- 1 Y. Li, R. Xu, Y. Ren, J. Lu, H. Wu, L. Wang, D. J. Miller, Y. K. Sun, K. Amine and Z. Chen, *Nano Energy*, 2016, **19**, 522–531.
- 2 S. T. Myung, F. Maglia, K. J. Park, C. S. Yoon, P. Lamp, S. J. Kim and Y. K. Sun, *ACS Energy Lett.*, 2017, **2**, 196–223.
- 3 S. Ahmed, P. A. Nelson, K. G. Gallagher, N. Susarla and D. W. Dees, *J. Power Sources*, 2017, **342**, 733–740.
- 4 G. Berckmans, M. Messagie, J. Smekens, N. Omar, L. Vanhaverbeke and J. Van Mierlo, *Energies*, 2017, **10**, 1314.
- 5 W. H. Ryu, J. Y. Eom, R. Z. Yin, D. W. Han, W. K. Kim and H. S. Kwon, *J. Mater. Chem.*, 2011, **21**, 15337–15342.
- 6 Z. Yang, W. Yang, D. G. Evans, Y. Zhao and X. Wei, *J. Power Sources*, 2009, **189**, 1147–1153.
- 7 A. Bhandari and J. Bhattacharya, *J. Electrochem. Soc.*, 2017, **164**, A106–A127.
- 8 M. Saulnier, A. Auclair, G. Liang and S. B. Schougaard, *Solid State Ionics*, 2016, **294**, 1–5.
- 9 J. Lu, C. Zhan, T. Wu, J. Wen, Y. Lei, A. J. Kropf, H. Wu, D. J. Miller, J. W. Elam, Y. K. Sun, X. Qiu and K. Amine, *Nat. Commun.*, 2014, **5**, 5693.
- 10 Y. Y. Xia, Y. H. Zhou and M. Yoshio, *J. Electrochem. Soc.*, 1997, **144**, 2593–2600.
- 11 K. Ragavendran, H. Xia, P. Mandal and A. K. Arof, *Phys. Chem. Chem. Phys.*, 2017, **19**, 2073–2077.
- 12 Y. Shang, X. Lin, X. Lu, T. Huang and A. Yu, *Electrochim. Acta*, 2015, **156**, 121–126.
- 13 F. D. Yu, Z. B. Wang, F. Chen, J. Wu, X. G. Zhang and D. M. Gu, *J. Power Sources*, 2014, **262**, 104–111.
- 14 K. Suryakala, G. P. Kalaignan and T. Vasudevan, *Mater. Chem. Phys.*, 2007, **104**, 479–482.
- 15 T. Kakuda, K. Uematsu, K. Toda and M. Sato, *J. Power Sources*, 2007, **167**, 499–503.
- 16 H. Zhao, S. Liu, Y. Cai, Z. Wang, M. Tan and X. Liu, *J. Alloys Compd.*, 2016, **671**, 304–311.
- 17 M. Chen, P. Chen, F. Yang, H. Song and S. Liao, *Electrochim. Acta*, 2016, **206**, 356–365.
- 18 R. Thirunakaran, A. Sivashanmugam, S. Gopukumar and R. Rajalakshmi, *J. Power Sources*, 2009, **187**, 565–574.
- 19 Z. Zhang, Z. Chen, G. Wang, H. Ren, M. Pan, L. Xiao, K. Wu, L. Zhao, J. Yang, Q. Wu, J. Shu, D. Wang, H. Zhang, N. Huo and J. Li, *Phys. Chem. Chem. Phys.*, 2016, **18**, 6893–6900.
- 20 J. Jiang, K. Du, Y. Cao, Z. Peng and G. Hu, *J. Nanosci. Nanotechnol.*, 2015, **15**, 421–425.
- 21 G. Xu, Z. Liu, C. Zhang, G. Cui and L. Chen, *J. Mater. Chem. A*, 2015, **3**, 4092–4123.
- 22 G. H. Waller, P. D. Brooke, B. H. Rainwater, S. Y. Lai, R. Hu, Y. Ding, F. M. Alamgir, K. H. Sandhage and M. L. Liu, *J. Power Sources*, 2016, **306**, 162–170.
- 23 A. Tron, Y. D. Park and J. Mun, *J. Power Sources*, 2016, **325**, 360–364.





- 24 J. Y. Shi, C. W. Yi and K. Kim, *J. Power Sources*, 2010, **195**, 6860–6866.
- 25 J. Zhao and Y. Wang, *J. Phys. Chem. C*, 2012, **116**, 11867–11876.
- 26 D. Guan, J. A. Jeevarajan and Y. Wang, *Nanoscale*, 2011, **3**, 1465–1469.
- 27 J. Zhao and Y. Wang, *Nano Energy*, 2013, **2**, 882–889.
- 28 C. G. Han, C. Zhu, G. Saito, N. Sheng, T. Nomura and T. Akiyama, *Electrochim. Acta*, 2017, **224**, 71–79.
- 29 J. Zeng, M. Li, X. Li, C. Chen, D. Xiong, L. Dong, D. Li, A. Lushington and X. Sun, *Appl. Surf. Sci.*, 2014, **317**, 884–891.
- 30 Y. Cho and J. Cho, *J. Electrochem. Soc.*, 2010, **157**, A625–A629.
- 31 M. G. Kim and J. Cho, *Adv. Funct. Mater.*, 2009, **19**, 1497–1514.
- 32 G. Zhou and L. Duan, *The basis of structural chemistry*, Peking university press, Beijing, 3rd edn, 2003, p. 312.
- 33 C. Q. Xu, Y. W. Tian, Y. C. Zhai and L. Y. Liu, *Mater. Chem. Phys.*, 2006, **98**, 532–538.

